



Raman Lidar Polly^{XT}:
the neXT generation

R. Engelmann et al.

EARLINET Raman Lidar Polly^{XT}: the neXT generation

R. Engelmann¹, T. Kanitz¹, H. Baars¹, B. Heese¹, D. Althausen¹, A. Skupin¹,
U. Wandinger¹, M. Komppula², I. S. Stachlewska³, V. Amiridis⁴, E. Marinou⁴,
I. Mattis⁵, H. Linné⁶, and A. Ansmann¹

¹Leibniz Institute for Tropospheric Research (TROPOS), Leipzig, Germany

²Finnish Meteorological Institute, Kuopio, Finland

³University of Warsaw, Faculty of Physics, Institute of Geophysics, Warsaw, Poland

⁴National Observatory of Athens, Athens, Greece

⁵Deutscher Wetterdienst, Meteorologisches Observatorium Hohenpeißenberg,
Hohenpeißenberg, Germany

⁶Max Planck Institute for Meteorology, Hamburg, Germany

Received: 24 June 2015 – Accepted: 30 June 2015 – Published: 24 July 2015

Correspondence to: R. Engelmann (ronny@tropos.de)

Published by Copernicus Publications on behalf of the European Geosciences Union.

Title Page

Abstract

Introduction

Conclusions

References

Tables

Figures



Back

Close

Full Screen / Esc

Printer-friendly Version

Interactive Discussion



Abstract

The atmospheric science community demands for autonomous and quality-assured vertically resolved measurements of aerosol and cloud properties. For this purpose, a portable lidar called Polly was developed at TROPOS in 2003. The lidar system was continuously improved with gained experience from EARLINET, worldwide field campaigns and institute collaborations within the last 10 years. Here we present recent changes of the setup of our portable multiwavelength Raman and polarization lidar Polly^{XT} and the improved capabilities of the system by means of a case study. Our latest developed system includes an additional near-range receiver unit for Raman measurements of the backscatter and extinction coefficient down to 120 m above ground, a water-vapor channel, and channels for simultaneous measurements of the particle linear depolarization at 355 and 532 nm. Quality improvements were achieved by following consequently the EARLINET guidelines and own developments. A modified ship radar ensures measurements in agreement with air-traffic safety regulations and allows 24/7 monitoring of the atmospheric state with Polly^{XT}.

1 Introduction

Lidar profiling of atmospheric aerosol and cloud layers has become important for climate research during the last decades. More recently, the volcanic eruption hazards of Eyjafjallajökull and Grimsvötn (Ansmann et al., 2010a; Tesche et al., 2012) for aircraft safety have shown the need for a height-resolved monitoring of the aerosol concentration on continental scales. This can be achieved either by spaceborne applications, e. g., with the Cloud-Aerosol Lidar and Infrared Pathfinder Satellite Observations mission (CALIPSO, Winker et al., 2009) or by networks of ground-based aerosol profilers as organized in the European Aerosol Research Lidar Network (EARLINET, Bösenberg and Hoff, 2008; Pappalardo et al., 2014) and the ceilometer network of the German Meteorological Service (DWD, Flentje et al., 2010). The disadvantage of the polar-orbiting

AMTD

8, 7737–7780, 2015

Raman Lidar Polly^{XT}: the neXT generation

R. Engelmann et al.

Title Page

Abstract

Introduction

Conclusions

References

Tables

Figures



Back

Close

Full Screen / Esc

Printer-friendly Version

Interactive Discussion



Raman Lidar Polly^{XT}: the neXT generation

R. Engelmann et al.

Title Page

Abstract

Introduction

Conclusions

References

Tables

Figures



Back

Close

Full Screen / Esc

Printer-friendly Version

Interactive Discussion



lidar aboard CALIPSO is the low temporal resolution, because it overpasses the same area only every 16th day. Ceilometer networks are operated 24/7, but are not able to distinguish aerosol particles in terms of their mean size, shape, or extinction efficiency. Within EARLINET, now part of the Aerosols, Clouds, and Trace gases Research InfraStructure (ACTRIS¹), aerosol and cloud profiling and characterization is performed with different Raman and polarization lidars three times per week. EARLINET members have developed lidar techniques and algorithms in order to harmonize the lidar measurements in Europe, to setup quality standards, to perform systematic test routines, and to improve data evaluation (e.g., Pappalardo et al., 2014; Freudenthaler et al., 2010; Freudenthaler, 2008). However, most of the lidar systems are prototypes leading to a huge variety of partly manually controlled system setups.

For more than ten years, at TROPOS the aim has been to develop smart, portable lidar systems (Polly) with the capabilities of advanced EARLINET lidars and EARLINET quality standards, but for stand-alone operation at remote places. In previous years, these systems were successfully used within EARLINET and showed also promising applicability for 24/7 operation at supersites combined with cloud-radar measurements, e.g., the Leipzig Aerosol and Cloud Remote Observations System (LACROS, Wandinger et al., 2012). An important advantage of the Polly systems is the uniform data structure and the easy-to-adjust software updates. All Polly lidars are operated within a network called PollyNET² (Althausen et al., 2013), which ensures data backup, instrument monitoring, and an international transfer of knowledge.

The very first Polly, a single-wavelength Raman lidar, was developed in 2003 (Althausen et al., 2009). Since then, further lidar systems along the line of Polly have been developed and permanently upgraded. Since 2006, two multi-wavelength Raman and polarization lidar systems with eXTended capabilities (Polly^{XT}) have been developed and operated by TROPOS and FMI. These systems enabled the determination of the particle backscatter coefficients at 355, 532, and 1064 nm and extinction coefficients

¹<http://www.actris.net>

²<http://polly.tropos.de>

**Raman Lidar Polly^{XT}:
the neXT generation**

R. Engelmann et al.

Title Page

Abstract

Introduction

Conclusions

References

Tables

Figures



Back

Close

Full Screen / Esc

Printer-friendly Version

Interactive Discussion



at 355 and 532 nm (therefore often called 3+2 lidars). The spectral backscatter and extinction coefficients allow for aerosol classification by optical properties of aerosol particles (Müller et al., 2007) and applying inversion algorithms (Müller et al., 1999; Baars et al., 2012) to derive the particle size distribution and concentration. In addition, a polarization-sensitive channel (+1) was installed to determine the shape of the aerosol particles from measurements of the (particle) linear depolarization ratio (Kanitz et al., 2013), to separate dust and non-dust particles in mixed aerosol layers (Baars et al., 2011), and to investigate mixed-phase clouds (Kanitz et al., 2011). In the framework of worldwide field campaigns these 3+2+1 Polly^{XT} systems achieved a unique lidar data set in the Amazonian basin, India, China, South Africa, Finland, Chile, and over the Atlantic aboard the research vessels POLARSTERN and METEOR. Figure 1 shows impressions from a selection of the very different measurement locations.

In 2009 and 2010, two additional Polly^{XT} lidars were developed with the setup described in Althausen et al. (2009). One has been operated stationary as a new EARLINET station (Preißler et al., 2013) at the Geophysics Centre of Évora (CGE, University of Évora, Portugal). The other one has been mounted at the meteorological monitoring station on Baengnyeong Island, Korea and has been operated by the Korean National Institute for Environmental Research (NIER).

In 2011, the Polly^{XT} systems of TROPOS and FMI underwent overall maintenance, upgrades of the optical setup, and were equipped with an additional water-vapor Raman channel (407 nm). In 2013, another two systems with two depolarization channels at 532 and 355 nm were setup in cooperation with the University of Warsaw (UW) and in the framework of the mobile sea facility OCEANET-Atmosphere (Kanitz et al., 2013). The latter includes a second receiver unit for the near range at 532 and 607 nm with a full overlap in 120 m above ground (Sect. 5.3) and an improved data acquisition unit (Sect. 2.3). In 2015, a similar near-range receiver with 4 channels (355, 387, 532, and 607 nm) was developed for the Polly^{XT}_UW system as well. Recently, two more systems following the UW and OCEANET design were finished and will be put into service at the National Observatory of Athens (NOA, Greece) and the Deutscher Wetterdienst

(DWD, Hohenpeißenberg, Germany), respectively. Table 1 gives an overview of the Polly^{XT} family and the capabilities of the various systems.

Since the system's presentation in 2009 (Althausen et al., 2009) the numerous improvements of Polly^{XT} build up a neXT generation of Polly^{XT}s that are the topic of the present paper. At the beginning of the paper, we give an overview about our latest developed system Polly^{XT}_OCEANET. Afterwards, we show recent improvements of Polly^{XT} in terms of an additional detection channel for water-vapor profiling (Sect. 3), adjustments in the optical setup to determine the particle linear depolarization ratio (Sect. 4), and achievements in the critical overlap range for lidar systems (Sect. 5). Finally, we present a case study of observed marine and dust layers from measurements aboard the research vessel METEOR to show the capabilities of the new generation of our smart Pollys. A conclusion and outlook section is given at the end.

2 Systems

2.1 Overview

Figure 2 presents the simple concept of our lidar. The Polly systems are housed in an outdoor cabinet or in case of Polly^{XT}_OCEANET in a container to allow the operation under various climatic conditions. The systems run autonomously by programmed measurement procedures and can be fully controlled by remote access via Internet. In case of rain events, measurements are automatically interrupted and resumed thereafter. When required by air-safety regulations the system can be attached to a modified FURUNO radar (Duck et al., 2005) in order to shut off the laser beam in case an airplane is detected in a $\pm 15^\circ$ cone above the lidar.

In terms of maintenance, the systems require much less attendance than many manually operated research Raman lidars used in EARLINET. The Pollys only need cleaning of the exit windows, if necessary, laser maintenance (flash lamp replacement) every three months, occasional realignment of the laser beam, and exchange of neutral-

Raman Lidar Polly^{XT}: the neXT generation

R. Engelmann et al.

Title Page

Abstract

Introduction

Conclusions

References

Tables

Figures



Back

Close

Full Screen / Esc

Printer-friendly Version

Interactive Discussion



density filters, if aerosol conditions change significantly. In extreme climatic conditions the internal heating has to be adapted.

Within PollyNET the development of an internal automatic data analysis was needed. At the web page of PollyNET automatically retrieved profiles of the backscatter and extinction coefficient are presented each 30 min, whenever atmospheric conditions have been appropriate. These developments have been made in parallel but also in consistency with the automatic software developments within the framework of EARLINET and ACTRIS. Promising results were achieved during previous tests (D'Amico et al., 2015). For EARLINET the Single Calculus Chain (SCC) has been developed to automate and harmonize the lidar data analysis within the network, while within PollyNET the data analysis benefits from the equal hardware and data format standards. The methodology and the results from the last 10 years of measurements within PollyNET will be presented in an upcoming publication currently in preparation (Baars et al., 2015).

2.2 Optical concept

Because it is the most complex Polly system so far, the optical setup of Polly^{XT}_OCEANET is presented in Fig. 3. In Polly^{XT}, the operated laser is an Inlite III from Continuum (Althausen et al., 2009). The laser emits light pulses at 1064 nm with a repetition frequency of 20 Hz. The position of the laser head in the optical setup is denoted by E1 in Fig. 3. The alignment of the laser beam through the external second and third harmonic generators (SHG, THG, E2 in Fig. 3) was improved by using a more rugged setup as well as by predefined adjustment apertures. After SHG and THG laser pulses of 180 mJ at 1064 nm, 110 mJ at 532 nm, and 60 mJ at 355 nm are emitted. The laser power is logged by means of an internal sensor during the measurements, and an external power meter (E2a) is used to measure solely the UV component in order to observe the conversion efficiency continuously for later quality control.

The purity of the linear polarization of the pulses at all wavelengths is subsequently ensured by the use of a waveplate and a Brewster-cut Glan-Laser polarizer (E3 in

Raman Lidar Polly^{XT}: the neXT generation

R. Engelmann et al.

Title Page

Abstract

Introduction

Conclusions

References

Tables

Figures



Back

Close

Full Screen / Esc

Printer-friendly Version

Interactive Discussion



**Raman Lidar Polly^{XT}:
the neXT generation**

R. Engelmann et al.

Title Page

Abstract

Introduction

Conclusions

References

Tables

Figures



Back

Close

Full Screen / Esc

Printer-friendly Version

Interactive Discussion



Fig. 3). Further explanation is given in Sect. 4.1. Via two dichroic mirrors the light is redirected upwards. In Fig. 3 E4 denotes an additional shutter. The shutter is controlled from a modified FURUNO ship radar and prohibits the emission of laser light during air-plane overflights. Finally, the 6 mm beam of the Inlite III is expanded to 45 mm diameter with a beam expander (E5 in Fig. 3) before the light is emitted into the atmosphere.

The far-range receiver unit of all Polly^{XT} systems includes a Newtonian telescope with a 300 mm primary mirror (R2 in Fig. 3). A device for the absolute calibration of the depolarization measurements is mounted in front of the pinhole (R3, see Sect. 4.3). The pinhole itself has a diameter of 0.9 mm. Thereafter, a lens pair collimates the received light. Dichroic beam splitters separate the radiation by wavelength. The laser-beam overlap with the receiving telescope is monitored with a triggered camera (CAM) that observes the beam at 532 nm. The pictures of the overlap serve for real time monitoring and are stored for long-term system performance analysis. The camera and all receiver channels are equipped with interference filters for background suppression (see Table 2 for detailed information). Planoconvex lenses in front of each photo multiplier tube (PMT) are used to project an image of the primary mirror onto the photo cathode in order to minimize influences of inhomogeneities of the sensitivity of the photo cathodes which can otherwise result in range-dependent deviations of the lidar signal (Simeonov et al., 1999; Freudenthaler, 2004).

Photon-counting is performed for all channels. Small PMT modules of Hamamatsu (type: P10721-110) are used for all wavelengths, except for the 1064 nm wavelength. Here, a Hamamatsu R3236 is applied which is cooled below -30°C with a multi-stage thermo-electric cooler (see Fig. 3).

Polly^{XT}_OCEANET includes an additional near-range receiver unit (R1, see Sect. 5.3) to lower the overlap-affected height range of the overall system to 120 m above the lidar, i. e., to decrease the minimal measurement height in the planetary boundary layer. In this way, better closure measurements in combination with in-situ measurements can be performed. Table 2 summarizes the general parameters of Polly^{XT}_OCEANET.

($< 5 \text{ Mcounts s}^{-1}$; Mcps) by applying neutral-density filters. Then, we perform the same measurement with higher maximum count rates ($> 100 \text{ Mcps}$). Figure 6 shows the result of such a measurement. The inset graph shows the two signals from the light ramps. The blue curve is obtained with a high light level and therefore flattened at the maximum. The black line was calculated from the measurement with less light but is scaled to linearly match the blue curve at low count rates from 0–10 Mcps.

The main graph shows the correlation between the two lines from the inset separated in the increasing (green) and decreasing (red) paths of the light ramp, respectively. Both paths are identical and show that no issues with after-pulsing or signal-induced noise effects are apparent. From this data it was found that the *paralyzable* theory is not always adequate for count rates higher than 40 Mcps and differences to such a model occur. Another typical issue with the correction according to the *paralyzable* theory is that it can only be solved iteratively and thus is time consuming. Therefore, the data in Fig. 6 was fitted by a 5th-order polynomial and the coefficients and their errors are stored in our raw-data files. In this way, correcting of the dead-time effects in our post-processing line is straightforward.

3 Water-vapor measurements

Operational aerosol lidar systems can be even more valuable, if they have the simultaneous capability to monitor the atmospheric water vapor. Water vapor is the most important greenhouse gas in the Earth's radiation budget and controls aerosol optical properties. Vertical profiles of the water-vapor mixing ratio can serve as input value for height-resolved radiative-transfer calculations, to investigate the hygroscopicity of aerosols, and the processes of cloud formation. The new setup of Polly includes an additional channel at 407 nm for the detection of Raman scattered light from water vapor (e.g. Wandinger, 2005). An automated calibration scheme by use of a microwave radiometer was recently presented in Foth et al. (2015).

Title Page

Abstract

Introduction

Conclusions

References

Tables

Figures



Back

Close

Full Screen / Esc

Printer-friendly Version

Interactive Discussion



**Raman Lidar Polly^{XT}:
the neXT generation**

R. Engelmann et al.

Title Page

Abstract

Introduction

Conclusions

References

Tables

Figures



Back

Close

Full Screen / Esc

Printer-friendly Version

Interactive Discussion



Figure 7 shows one of the first measurements of the water-vapor mixing ratio with Polly^{XT}_TROPOS. The measurement took place at Leipzig on 10 February 2012 from 19:00 to 20:30 UTC. The comparison with a co-located radiosonde launch and with the EARLINET Raman lidar MARTHA (Multiwavelength Aerosol Raman Lidar for Temperature, Humidity, and Aerosol profiling, 80 cm telescope, 350 mJ at 355 nm, 30 Hz, Mattis et al., 2002) shows very good agreement, even under these relatively dry conditions with less than 1.5 g kg^{-1} of water vapor in the planetary boundary layer. The difference between the two lidar measurements is less than 0.2 g kg^{-1} up to 5 km height (30 m height resolution). Somewhat larger differences between lidar and radiosonde data might be caused by the drift-off of the sonde.

The presented data were obtained from a night-time measurement. The low Raman scattering cross section of water vapor does not allow measurements during daytime with the current Polly setup. Moreover, the water-vapor detector is automatically switched off during daytime, because the daylight background intensity can be near the damage threshold of the PMT.

4 Determination of particle linear depolarization ratio

The linear depolarization ratio has gained importance for aerosol and cloud layer separation (Liu et al., 2010), as well as cloud and aerosol type identification (Sassen, 2005; Omar et al., 2009). In addition, the particle linear depolarization ratio is well suited to characterize aerosol particles (Freudenthaler et al., 2009; Preißler et al., 2013) and to separate dust and non-dust particles mixed aerosol layers (Teschke et al., 2009; Ansmann et al., 2010b; Baars et al., 2012; Kanitz et al., 2013). Even fine and coarse-mode dust can be separated by means of polarization lidar and Sun photometer measurements (Mamouri and Ansmann, 2014). These approaches require measurements of depolarized light with high accuracy.

Moreover, measurements of the particle linear depolarization ratio at two different wavelengths simultaneously can help to study aerosol mixtures and separate their

components. The spectral slope of the aerosol depolarization is sensitive to the ratio of the fine and coarse mode of non-spherical particles (Sakai, 2010; Burton et al., 2012).

4.1 Laser polarization

The linear depolarization ratio of Rayleigh scattering is smaller than 1.5% in dependence of the width of the used interference filters (Behrendt and Nakamura, 2002). In case of Polly^{XT} (filter width of 1.0 nm) molecular linear depolarization ratios of 0.75 and 0.53% are expected at 355 and 532 nm, respectively, assuming 100% purity of the linearly polarized emitted laser light. The purity of linear polarization of typical flash-lamp-pumped and Q-switched Nd:YAG laser systems at the fundamental wavelength is about 98 to 99%. Birefringence in the laser rod usually induces small amounts of cross-polarized light.

In contrast, the generation of second and third harmonic radiation can significantly decrease the purity of polarization and affect the accuracy of measurements. SHG and THG are both of type II in the current Polly^{XT} setup, i.e., the radiation at 355, 532, and 1064 nm is vertically, horizontally, and elliptically polarized, respectively, with respect to the optical board. A common approach to purify the linear polarization of the laser light is to separate the beams, polarize them, and afterwards recombine the beams onto one axis or even transmit the beams separately. In contrast, we implemented a multiwavelength polarizer setup without prior beam separation for a convenient beam alignment, for stability, and for combined beam expansion afterwards. Figure 8 shows the approach to generate highly polarized light from the three Nd:YAG wavelengths. A quartz-crystal wave plate with different retardations at the three fundamental wavelengths was manufactured (Bernhard Halle Nachfl. GmbH, Berlin, Germany) in order to rotate the polarization plane at 532 nm (2.5λ) but not at 355 nm (4λ). At 1064 nm (1.2λ) the light is elliptically polarized and by inserting the wave plate either at $+45^\circ$ or -45° the vertically polarized component can be maximized. After the wave plate a Brewster-cut Glan-Laser polarizer (Artifex Engineering, Emden, Germany) is inserted which pro-

Raman Lidar Polly^{XT}: the neXT generation

R. Engelmann et al.

Title Page

Abstract

Introduction

Conclusions

References

Tables

Figures



Back

Close

Full Screen / Esc

Printer-friendly Version

Interactive Discussion



vides an extinction ratio of $< 5 \times 10^{-5}$ over a wavelength range from 350–2300 nm with an angular beam separation of < 0.01 mrad. Hence, the polarization impurity of the transmitted laser beam is well below 0.1 % and sufficiently low for depolarization measurements in terms of EARLINET standards.

5 4.2 Polarization effects of beam splitters

Dichroic beam splitters show different transmissions for parallel and cross-polarized (p and c-polarized) light which results in different transmission efficiencies for both polarization states at each detection channel. Mattis et al. (2009) showed systematic errors of lidar signals because of polarization-dependent receiver efficiencies in the presence of depolarizing aerosols, which can result in discrepancies of > 60 % in the total particle backscatter coefficient. Overcoming this bias is possible, if the volume linear depolarization ratio (δ^v) at the respective wavelength as well as the receiver transmission ratios

$$R_i = \frac{\eta_{i,c}}{\eta_{i,p}} \quad (1)$$

are known for the channels i . Here, $\eta_{i,c}$ and $\eta_{i,p}$ denote the detection efficiency of a channel for cross and parallel-polarized light with respect to the laser polarization plane. With these parameters the corrected lidar signals $P_{i,\text{corr}}$ can be calculated from the measured signal P_i (Mattis et al., 2009):

$$P_{i,\text{corr}} = P_i \frac{1 + R_i \delta^v}{1 + \delta^v}. \quad (2)$$

In principle, a good polychromator design should result in values of R_i of about 1 for the total elastic-backscatter channels so that the former correction does not induce significant errors and might be even not necessary. In turn, high values of R_i (> 500) are desired for the polarization-sensitive channels. For Raman channels R_i is negligible

Title Page

Abstract

Introduction

Conclusions

References

Tables

Figures

◀

▶

◀

▶

Back

Close

Full Screen / Esc

Printer-friendly Version

Interactive Discussion



since the molecular depolarization is nearly constant with height and changes only slightly with temperature in dependence of the width of the applied interference filter in these channels.

Although the remaining bias from non-ideal beam splitters can be corrected with Eq. (2), it yields another step in the data evaluation and can increase the overall errors. Under this consideration, several beam splitters were substituted in the TROPOS and FMI Polly^{XT}s during the upgrade. The obtained values for the newest design of Polly are satisfactory and show generally a sensitivity difference of each channel for parallel and cross-polarized light below 10%. Table 4 gives an overview on the actual values of R_j .

A suitable way to determine R_j is to use an artificial light source with a polarizer in front. In this way, the receiver efficiencies can be measured in dependence of the incident polarization plane and R_j can be obtained. We use a fiber-coupled halogen (visible and near-infrared radiation) and deuterium (ultraviolet radiation) lamp, a collimator lens, and a Glan–Taylor polarizer in a motorized rotation mount. The device is then mounted in front of the receiver telescope and the measurements of the relative receiver efficiencies are performed.

4.3 Calibration of the linear depolarization ratio

Depolarization measurements are performed with all Polly^{XT} systems (Table 1) at 532 nm and partly at 355 nm, too. In the past, the Rayleigh calibration method was applied within the data analysis under the assumption of pure Rayleigh depolarization in an aerosol-free height range (Behrendt and Nakamura, 2002). However, this method includes large uncertainties (e.g., Reichardt, 2003).

An alternative method is the $\Delta 90^\circ$ -calibration (formerly known as $\pm 45^\circ$ -calibration, Freudenthaler et al., 2009). In order to include this method to the automatic measurement procedure of Polly a remote-controlled rotary mount with a polarizer close to the focal plane of the receiver telescope was added to the system. This sheet polarizer (LPG23, company ITOS, Mainz, Germany) is equipped with a decentered hole to mea-

Title Page

Abstract

Introduction

Conclusions

References

Tables

Figures

◀

▶

◀

▶

Back

Close

Full Screen / Esc

Printer-friendly Version

Interactive Discussion



Raman Lidar Polly^{XT}:
the neXT generation

R. Engelmann et al.

Title Page

Abstract

Introduction

Conclusions

References

Tables

Figures

◀

▶

◀

▶

Back

Close

Full Screen / Esc

Printer-friendly Version

Interactive Discussion



sure without the polarizer in the light path in normal mode by rotating the hole onto the optical axis. Three times per day, the polarizer is rotated under $+45^\circ$ and -45° with respect to the laser polarization plane in the light path for calibration. In this way, the volume linear depolarization ratio δ^v from the ratio $\delta' = P_c/P_t$ of the cross-polarized (c) and the total (t) signal is given by

$$\delta^v = \frac{1 - \delta'/C}{\delta'R_t/C - R_c}, \quad (3)$$

with the absolute calibration

$$C = \frac{1 + R_t}{1 + R_c} \sqrt{\delta'_{+45} \delta'_{-45}}, \quad (4)$$

following Freudenthaler et al. (2009). The transmission ratios R for total and cross-polarized radiation were determined as explained in Sect. 4.2. Figure 9 shows the time series of the determined calibration constant C during routine measurements of Polly^{XT}_IFT. The constant shows rather stable values except for changes during setting adjustments. For the period from 07 August to 19 October 2012 C was 0.090 ± 0.004 , from 19 October to 14 November 2012 0.170 ± 0.008 , and from 20 December 2012 to 07 March 2013 $0.080 \pm 0.01\%$. The higher variability in the last period is based on short-time changes in the settings. At the end of November 2012 the fluctuations are caused by low signal-to-noise ratios.

5 Optimization of measurement range

Polly^{XT} was designed to measure primarily tropospheric aerosols which occur in their highest concentration close to the surface. Hence, certain optical design rules had to be considered. The most critical points concerned the laser beam stability and adjustment, the overlap function, and near-range performance. The latest type of Polly^{XT} is operated aboard the research vessels POLARSTERN and METEOR within the OCEANET

**Raman Lidar Polly^{XT}:
the neXT generation**

R. Engelmann et al.

Title Page

Abstract

Introduction

Conclusions

References

Tables

Figures



Back

Close

Full Screen / Esc

Printer-friendly Version

Interactive Discussion



project. Data coverage of the shallow marine boundary layer and the free troposphere is needed for studying dust fluxes, the exchange processes between the PBL and the free troposphere, and for comparison with ground-based in-situ measurements. Therefore, measurements are desired from 100 m height up to the tropopause in the marine environment.

5.1 Beam expansion and overlap adjustment

Beam expansion is performed to increase the pointing stability and to reduce the divergence of the laser beam which was specified to be < 1.5 mrad. For Polly^{XT} the 6 mm beam of the Inlite-III laser is expanded to 45 mm (factor of 8) by a single achromatic beam expander after SHG and THG (E5 in Fig. 3), which reduces the full-angle laser beam divergence to < 0.2 mrad. This value is sufficiently small with respect to the field of view of the receiver telescope of 1.0 mrad.

The beam expander consists of three different lens materials for chromatic and spherical correction at the three wavelengths. The design was achieved by optimization calculation with the optical-design software ZEMAX and is given in Table 5.

In the setup of the lidar the overlap adjustment is performed within the expander, too. The beam can be aligned by transversely shifting the achromatic lens pair (objective) of the beam expander by using two stepper motors (Engelmann and Althausen, 2014). ZEMAX calculations showed that the beam can be tilted by 3–5 mrad without reducing the beam quality, i.e., without increasing the beam divergence above 0.2 mrad. In this way, no further optical steering elements have to be placed after the beam expander.

5.2 Overlap function

Tropospheric aerosol observations with lidar shall provide profiles of the extinction coefficient from the PBL to the tropopause. At low altitudes the measured signals are corrupted until the overlap function becomes unity.

**Raman Lidar Polly^{XT}:
the neXT generation**

R. Engelmann et al.

Title Page

Abstract

Introduction

Conclusions

References

Tables

Figures



Back

Close

Full Screen / Esc

Printer-friendly Version

Interactive Discussion



In contrast, the height of complete overlap cannot be arbitrarily low because of the strong dynamic increase of the signal towards the ground (with $1/r^2$ for a range r) which cannot be covered by the detectors and data acquisition. From EARLINET workshops in the past years it emerged that such a compromise to cover measurements in the entire troposphere with only one receiver telescope is almost impossible. Therefore, it became common practice to operate different receiver telescopes for different altitude ranges. Considering the requirements for a compact and easy to transport lidar system, an additional near-range telescope has been included in the latest design of Polly^{XT} (see Sect. 5.3). The far-range and primary receiver of the system was designed in such a way that the overlap function of the telescope reaches unity at 800–900 m but still can obtain a sufficient signal-to-noise ratio in the higher troposphere in order to calibrate the signals in aerosol-free air close to the tropopause region.

For measurements of quantities that are determined from signal ratios (backscatter coefficient by Raman method, linear depolarization, water-vapor mixing ratio) the height of complete overlap is not as essential as the equality of the overlap function for the separate detection channels. Therefore, extreme care was taken to guarantee that the optical paths behind the field stop are similar and the spread of incident angles of the radiation is less than 1° at the interference filters. The primary mirror is optically imaged onto the photocathodes of the PMTs to prevent height-dependent receiver efficiencies because of detector-surface inhomogeneities.

5.3 Near-range receiver

In order to fulfill the near-range profiling requirements with Polly^{XT}, a separate 50 mm refracting telescope was included in the design at a close distance of 120 mm from the axis of the laser beam. The conducted near-range observations can be used independently for the lidar data analysis, but provide another chance for data quality control and overlap determination of the far-range receiver as well. The refracting telescope consists of an achromatic lens (Thorlabs, AC508-250-A) with a focal length of 250 mm. A 550 μm fiber forms the field stop and transports the light. The field of view of the

**Raman Lidar Polly^{XT}:
the neXT generation**

R. Engelmann et al.

Title Page

Abstract

Introduction

Conclusions

References

Tables

Figures

I◀

▶I

◀

▶

Back

Close

Full Screen / Esc

Printer-friendly Version

Interactive Discussion



near-range receiver is 2.2 mrad, and the region of complete overlap was calculated by simulations to be at approximately 120 m. A fiber-optic scrambler using a Fourier lens (Arshinov et al., 2004) has been included in order to remove range-dependent angular distributions of the light when it exits the fiber and passes the adjacent beam separation and interference filters. The scrambler consists of a sapphire ball lens (personal communication, I. Serikov, 2012) of 2 mm diameter which directly links two fiber patch cables (Thorlabs, M37L02). Afterwards, the light passes a dichroic beam splitter and neutral-density and interference filters before the signals are detected at 532 and 607 nm.

Figure 10 shows the simulated and experimentally determined (Wandinger and Ansmann, 2002) overlap functions for the far-range and near-range receiving telescopes. Simulation and experimental result fit as expected and thus show a proper alignment of the system. The particle backscatter coefficient at 532 nm is also shown for the far and near range. The correction of the overlap function was not performed in order to show the measurement differences arising from the two telescopes.

6 Case study onboard of RV *Meteor*

A detailed analysis of all optical parameters which can be retrieved with Polly^{XT}_OCEANET is presented in Fig. 11. In May 2013 the German research vessel METEOR performed an Atlantic transect cruise at 14.5° N from the Caribbean island of Guadeloupe to the Cape Verde island of Mindelo. The lidar was operated continuously during the cruise in order to study Saharan dust during its transport westward to Central America (Kanitz et al., 2014). On 09 May 2013 about 3000 km from the West African coast (14.5° N, 44.1° W) the first Saharan dust plume was observed. The layer extended from 1.7 to 3.4 km height with maximum extinction coefficients of 80 and 75 Mm⁻¹ at 355 and 532 nm, respectively. The aerosol optical depth of the dust layer was approximately 0.07 ± 0.01 at 532 nm.

**Raman Lidar Polly^{XT}:
the neXT generation**

R. Engelmann et al.

Title Page

Abstract

Introduction

Conclusions

References

Tables

Figures



Back

Close

Full Screen / Esc

Printer-friendly Version

Interactive Discussion



Polly allows us to measure particle backscatter coefficients at three wavelengths (Fig. 11a) and the corresponding backscatter-related Ångström exponents (Ångström, 1964) with very high vertical resolution. The backscatter-related Ångström exponents describe the spectral dependence of the backscatter coefficients (Fig. 11d, thick blue and red curves). Furthermore, the climate-relevant particle extinction coefficients at 355 and 532 nm are determined with the Raman lidar method (Ansmann et al., 1992; Ansmann and Müller., 2005) as well as the corresponding extinction-related Ångström exponent (Fig. 11d, thin blue curve). From the 355 and 532 nm backscatter and extinction coefficients the extinction-to-backscatter ratios (lidar ratios) are computed (shown in Fig. 11c). Together with the particle depolarization ratios in Fig. 11e and the Ångström exponents in Fig. 11d, the lidar ratios serve as a basis for an unambiguous aerosol typing (Müller et al., 2007; Tesche et al., 2011; Burton et al., 2012; Groß et al., 2013).

Lidar ratios of 50 ± 5 (for 355 nm) and 39 ± 5 sr (for 532 nm) in the lofted dust plume at 2–3 km height together with particle linear depolarization ratios around 0.16 ± 0.02 and 0.175 ± 0.01 at 355 and 532 nm, respectively, and extinction-related Ångström exponents of 0.65 ± 0.2 indicate an aged dust plume mixed with biomass-burning aerosol originating from fires in the African tropical belt (Tesche et al., 2011; Ansmann et al., 2009). Pure Saharan dust plumes caused extinction-related Ångström exponents of 0.0 ± 0.2 after Tesche et al. (2009). The interpretation of the backscatter-related Ångström exponents is complicated by the fact that dust particles are irregularly shaped and shape-related optical effects are different for different wavelengths (Gasteiger et al., 2011). However, in combination with the other optical parameters we conclude that the low backscatter-related 355/532 nm Ångström exponents of -0.01 ± 0.17 indicate comparably large smoke particles mixed with dust. According to Müller et al. (2007), smoke particles grow during transport by water uptake.

The aged lofted plume is well mixed (after the transport of 3000–5000 km from Africa according to backward trajectories) as the almost height-independent water-vapor mixing ratio (Fig. 11f) indicates. For the relative humidity we obtained values of 40 % at

2 km height up to 60 % at 3 km from radiosondes launched aboard METEOR which again indicates a continental African origin of the airmass.

Below the pronounced dust/smoke plume, the surface-near layer contains a mixture of dust (turbulent downward mixing and sedimentation), aged smoke, and marine particles. Spherical particles (marine and smoke) dominated here and cause a particle linear depolarization ratio of < 0.05 at heights below 1 km. Comparably low lidar ratios of 20 ± 10 sr and Ångström exponents around 1 also indicate a mixture of these particle components. The water-vapor mixing ratio is almost height independent in the lowest 500 m, where also the 532 nm backscatter coefficient (from near-range and far-range channels) indicates well-mixed conditions, but decreases with height as a result of mixing of drier free-tropospheric with humid boundary-layer air.

A detailed analysis of the two-wavelength depolarization-ratio profiles will allow us to quantify the contribution of marine particles, smoke, fine-mode and coarse-mode dust to the observed optical properties (Mamouri and Ansmann, 2014). The METEOR cruise lasted from 28 April to 23 May 2013. Based on measurements shown in Fig. 11, a detailed characterization of dust/smoke/marine particle plumes in terms of optical and derived microphysical particle properties will be performed and afterwards compared to products obtained with atmospheric circulation models. Kanitz et al. (2014) showed already first intercomparisons of an ongoing analysis.

7 Current developments and outlook

In the last decade a simple Raman lidar prototype was further developed to a smart, automated multiwavelength Raman and polarization lidar with two receiver units and 3+2+2+2+1 capabilities (backscatter, extinction, depolarization, near-range telescope, and water vapor). The system combines latest EARLINET lidar quality standards in a stand-alone design. Until now, nine Polly systems exist. Two additional systems will be built for TROPOS in the near future. One will supplement our mobile LACROS facility and the second lidar will be permanently installed at the Cape Verde Atmo-

Title Page

Abstract

Introduction

Conclusions

References

Tables

Figures



Back

Close

Full Screen / Esc

Printer-friendly Version

Interactive Discussion



**Raman Lidar Polly^{XT}:
the neXT generation**

R. Engelmann et al.

Title Page

Abstract

Introduction

Conclusions

References

Tables

Figures



Back

Close

Full Screen / Esc

Printer-friendly Version

Interactive Discussion



spheric Observatory, Mindelo. The constant distribution of the idea of Polly may result in a small network of lidar stations around the world with unified systems and unified data analysis along the line of the Aerosol Robotic Network (AERONET). Up to now, all Polly measurements are collected within PollyNET and quicklooks of the data products are available for the scientific community and the general public in near-real time (<http://polly.tropos.de>). In this way, aerosol transport models can be potentially validated online or even assimilate the data and benefit from PollyNET. Furthermore, the data can be used for ground truthing of current and upcoming satellite missions.

The Polly systems have been continuously improved over the last 10 years and the progress is ongoing. Current ideas include a variety of quality-improving setup changes. For example, it is planned to automate the telecover test (Freudenthaler, 2008) and implement the test in the measurement schedule. In addition, the system is applied more and more for the investigation of aerosol-cloud interactions. An interesting approach with lidar was presented by Schmidt et al. (2013), called the dual-field-of-view technique, which might be installed in a Polly as well. Also doubling the number of photomultipliers to adjust the photon count rates for the weak aerosol backscatter on the one hand and for the strong backscatter of cloud particles on the other hand will be attempted. The colleagues from the University of Warsaw want to expand the near-range measurements to four channels to investigate the spectral behavior of absorbing aerosols in the planetary boundary layer and to enhance the overlap between ground-based remote sensing and in-situ measurements. The network of fully autonomous Polly systems with its near-real-time observing capabilities is expected to play an increasing role in the establishment of a long-term, sustainable research infrastructure for aerosol and cloud profiling in the framework of ACTRIS.

Acknowledgements. We are deeply grateful to Volker Freudenthaler, who spends endless working hours to unify and improve the quality of lidar systems in EARLINET and ACTRIS, for the outstanding collaboration. We also want to thank our collaboration partners for their confidence in our work and for their positive feedback. No Polly would exist without the outstanding effort of the TROPOS workshops and administration, first of all Conny Kurze and Ingolf Bernhardt. The research leading to these results has received funding from the European Union

Seventh Framework Programme (FP7/2007–2013) under grant agreement n° 262254 and in the framework of BEYOND (funded under: FP7-REGPOT-2012-2013-1) under grant agreement no. 316210.

References

- 5 Althausen, D., Engelmann, R., Baars, H., Heese, B., Ansmann, A., Müller, D., and Komppula, M.: Portable Raman lidar Polly^{XT} for automated profiling of aerosol backscatter, extinction, and depolarization, *J. Atmos. Ocean. Tech.*, 26, 2366–2378, doi:10.1175/2009JTECHA1304.1, 2009. 7739, 7740, 7741, 7742
- 10 Althausen, D., Engelmann, E., Baars, H., Heese, B., Kanitz, T., Komppula, M., Giannakaki, E., Pfüller, A., Silva, A. M., Preißler, J., Wagner, F., Rascado, J. L., Pereira, S., Lim, J. H., Ahn, J. Y., Tesche, M., and Stachlewska, I. S.: PollyNET – a network of multiwavelength polarization Raman lidars, in: *Proc. SPIE 8894, Lidar Technologies, Techniques, and Measurements for Atmospheric Remote Sensing IX*, 88940I, 22 October 2013, Dresden, Germany, 8894-17, doi:10.1117/12.2028921, 2013. 7739
- 15 Ångström, A.: The parameters of atmospheric turbidity, *Tellus*, 16, 64–75, doi:10.1111/j.2153-3490.1964.tb00144.x, 1964. 7755
- Ansmann, A. and Müller, D.: Lidar and atmospheric aerosol particles, in: *Lidar – Range-Resolved Optical Remote Sensing of the Atmosphere*, edited by: Weitkamp, C., Springer Series in Optical Sciences, New York, 105–141, doi:10.1007/0-387-25101-4_4, 2005. 7755
- 20 Ansmann, A., Wandinger, U., Riebesell, M., Weitkamp, C., and Michaelis, W.: Independent measurement of extinction and backscatter profiles in cirrus clouds by using a combined Raman elastic-backscatter lidar, *Appl. Optics*, 31, 7113–7131, doi:10.1364/AO.31.007113, 1992. 7755
- 25 Ansmann, A., Baars, H., Tesche, M., Müller, D., Althausen, D., Engelmann, R., Pauliquevis, T., and Artaxo, P.: Dust and smoke transport from Africa to South America: lidar profiling over Cape Verde and the Amazon rainforest, *Geophys. Res. Lett.*, 36, L11802, doi:10.1029/2009GL037923, 2009. 7755
- 30 Ansmann, A., Tesche, M., Groß, S., Freudenthaler, V., Seifert, P., Hiebsch, A., Schmidt, J., Wandinger, U., Mattis, I., Müller, D., and Wiegner, M.: The 16 April 2010 major volcanic ash plume over central Europe: EARLINET lidar and AERONET photome-

Raman Lidar Polly^{XT}: the neXT generation

R. Engelmann et al.

Title Page

Abstract

Introduction

Conclusions

References

Tables

Figures



Back

Close

Full Screen / Esc

Printer-friendly Version

Interactive Discussion



**Raman Lidar Polly^{XT}:
the neXT generation**

R. Engelmann et al.

Title Page

Abstract

Introduction

Conclusions

References

Tables

Figures



Back

Close

Full Screen / Esc

Printer-friendly Version

Interactive Discussion



ter observations at Leipzig and Munich, Germany, *Geophys Res. Lett.*, 371, L13810, doi:10.1029/2010GL043809, 2010a. 7738

Ansmann, A., Tesche, M., Seifert, P., Groß, S., Freudenthaler, V., Apituley, A., Wilson, K. M., Serikov, I., Linné, H., Heinold, B., Hiesch, A., Schnell, F., Schmidt, J., Mattis, I., Wandinger, U., and Wiegner, M.: Ash and fine-mode particle mass profiles from EARLINET-AERONET observations over central Europe after the eruptions of the Eyjafjallajökull volcano in 2010, *Geophys. Res. Lett.*, 116, D00U02, doi:10.1029/2010JD015567, 2010b. 7747

Arshinov, Y., Bobrovnikov, S., Serikov, I., Althausen, D., Ansmann, A., and Mattis, I.: Optic-fiber scramblers and a fourier transform lens as a means to tackle the problem on the overlap factor of LIDAR, in: 22nd International Laser Radar Conference (ILRC 2004). Proceedings of the Conference held 12–16 July, 2004 in Matera, Italy, edited by: Pappalardo, G. and Amodeo, A., ESA SP-561, European Space Agency, Paris, 227–230, 2004. 7754

Baars, H., Ansmann, A., Engelmann, R., and Althausen, D.: Continuous monitoring of the boundary-layer top with lidar, *Atmos. Chem. Phys.*, 8, 7281–7296, doi:10.5194/acp-8-7281-2008, 2008.

Baars, H., Ansmann, A., Althausen, D., Engelmann, R., Artaxo, P., Pauliquevis, T., and Souza, R.: Further evidence for significant smoke transport from Africa to Amazonia, *Geophys. Res. Lett.*, 382, L20802, doi:10.1029/2011GL049200, 2011. 7740

Baars, H., Ansmann, A., Althausen, D., Engelmann, R., Heese, B., Müller, D., Artaxo, P., Paixao, M., Pauliquevis, T. M., and Souza, R.: Aerosol profiling with lidar in the Amazon Basin during the wet and dry season, *J. Geophys. Res.*, 117, D21201, doi:10.1029/2012JD018338, 2012. 7740, 7747

Baars, H., Kanitz, T., Engelmann, R., Althausen, D., Heese, B., Kompulla, M., Preißler, J., Ansmann, A., Wandinger, U., Lim, J.-H., Ahn, J. Y., Stachlewska, I. S., Tesche, M., Amiridis, V., Marinou, E., Seifert, P., Hofer, J., Skupin, A., Schneider, F., Bohlmann, S., Foth, A., Bley, S., Pfüller, A., Giannakaki, E., Lihavainen, H., Viisanen, Y., Hooda, R. K., Pereira, S., Bortoli, D., Wagner, F., Janicka, L., Markowicz, K. M., Achtert, P., Artaxo, P., Pauliquevis, T., Souza, R., Sharma, V. P., van Zyl, P. G., Beukes, J. P., Sun, J., Casiccia, C., Rohwer, E. G., Deng, R., and Mamouri, R. E.: PollyNET: A network of automated Raman-polarization lidars for global aerosol profiling, to be submitted to *Atmos. Chem. Phys. Discuss.*, 2015. 7742

Behrendt, A. and Nakamura, T.: Calculation of the calibration constant of polarization lidar and its dependency on atmospheric temperature, *Opt. Express*, 10, 805–817, 2002. 7748, 7750

**Raman Lidar Polly^{XT}:
the neXT generation**

R. Engelmann et al.

Title Page

Abstract

Introduction

Conclusions

References

Tables

Figures



Back

Close

Full Screen / Esc

Printer-friendly Version

Interactive Discussion



Bösenberg, J. and Hoff, R.: Plan for the implementation of the GAW aerosol lidar observation network GALION, World Meteorological Organization Rep., Hamburg, Germany, 178, 53 pp., 2008. 7738

Burton, S. P., Ferrare, R. A., Hostetler, C. A., Hair, J. W., Rogers, R. R., Obland, M. D., Butler, C. F., Cook, A. L., Harper, D. B., and Froyd, K. D.: Aerosol classification using airborne High Spectral Resolution Lidar measurements – methodology and examples, *Atmos. Meas. Tech.*, 5, 73–98, doi:10.5194/amt-5-73-2012, 2012. 7748, 7755

D’Amico, G., Amodeo, A., Baars, H., Biniotoglou, I., Freudenthaler, V., Mattis, I., Wandinger, U., and Pappalardo, G.: EARLINET Single Calculus Chain – general presentation methodology and strategy, *Atmos. Meas. Tech. Discuss.*, 8, 4973–5023, doi:10.5194/amtd-8-4973-2015, 2015. 7742

Donovan, D. P., Whiteway, J. A., and Carswell, A. I.: Correction for nonlinear photon-counting effects in lidar systems, *Appl. Optics*, 32, 6742–6753, doi:10.1364/AO.32.006742, 1993. 7745

Duck, T., Firanski, B., Lind, F., and Sipler, D.: Aircraft-protection radar for use with atmospheric lidars, *Appl. Optics*, 44, 4937–4945, doi:10.1364/AO.44.004937, 2005. 7741

Engelmann, R. and Althausen, D.: Lidar system including an optical device with a transmitter and a receiver, EU Patent EP2172790 B1, EPAB European Patent Applications and Specifications, Munich, Germany, 2014. 7752

Flentje, H., Heese, B., Reichardt, J., and Thomas, W.: Aerosol profiling using the ceilometer network of the German Meteorological Service, *Atmos. Meas. Tech. Discuss.*, 3, 3643–3673, doi:10.5194/amtd-3-3643-2010, 2010. 7738

Foth, A., Baars, H., Di Girolamo, P., and Pospichal, B.: Water vapour profiles from Raman lidar automatically calibrated by microwave radiometer data during HOPE, *Atmos. Chem. Phys. Discuss.*, 15, 6567–6599, doi:10.5194/acpd-15-6567-2015, 2015. 7746

Freudenthaler, V.: Effects of spatially inhomogeneous photomultiplier sensitivity on LIDAR signals and remedies, in: *Proceedings of the 22nd International Laser Radar Conference (ILRC 2004)* held 12–16 July, 2004 in Matera, Italy, edited by: Pappalardo, G. and Amodeo, A., European Space Agency, Paris, 37 pp., ESA SP-561, 2004. 7743

Freudenthaler, V.: The telecover test: a quality assurance tool for the optical part of a lidar system, in: *Reviewed and Revised Papers Presented at the 24th International Laser Radar Conference*, Boulder, Colorado, USA, 23–27 June 2008, Boulder, Colorado, USA, presentation: S01P-30, available at: <http://epub.ub.uni-muenchen.de/12958/> (last access: 20 April 2015), 2008. 7739, 7757

**Raman Lidar Polly^{XT}:
the neXT generation**

R. Engelmann et al.

Title Page

Abstract

Introduction

Conclusions

References

Tables

Figures



Back

Close

Full Screen / Esc

Printer-friendly Version

Interactive Discussion



Freudenthaler, V., Esselborn, M., Wiegner, M., Heese, B., Tesche, M., Ansmann, A., Müller, D., Althausen, D., Wirth, M., Fix, A., Ehret, G., Knippertz, P., Toledano, C., Gasteiger, J., Garhammer, M., and Seefeldner, M.: Depolarization ratio profiling at several wavelengths in pure Saharan dust during SAMUM 2006, *Tellus B*, 61, 165–179, doi:10.1111/j.1600-0889.2008.00396.x, 2009. 7747, 7750, 7751

Freudenthaler, V., Groß, S., Engelmann, R., Mattis, I., Wandinger, U., Pappalardo, G., Amodeo, A., Giunta, A., D'Amico, G., Chaikovskiy, A., Osipenko, F., Slesar, A., Nicolae, D., Belegante, L., Talianu, C., Serikov, I., Linne, H., Jansen, F., Wilson, K., de Graaf, M., Apituley, A., Trickl, T., Giehl, H., and Adam, M.: EARLI09 – direct intercomparison of eleven EARLINET lidar systems, in: *Proceedings of the 25th International Laser Radar Conference*, 5–9 July 2010, St.-Petersburg, Russia, ISBN978-5-94458-109-9, 891–894, 2010. 7739

Gasteiger, J., Wiegner, M., Groß, S., Freudenthaler, V., Toledano, C., Tesche, M., and Kandler, K.: Modelling lidar-relevant optical properties of complex mineral dust aerosols, *Tellus B*, 63, 725–741, doi:10.1111/j.1600-0889.2011.00559.x, 2011. 7755

Groß, S., Esselborn, M., Weinzierl, B., Wirth, M., Fix, A., and Petzold, A.: Aerosol classification by airborne high spectral resolution lidar observations, *Atmos. Chem. Phys.*, 13, 2487–2505, doi:10.5194/acp-13-2487-2013, 2013. 7755

Johnson, F. A., Jones, R., McLean, T. P., and Pike, E. R.: Dead-time corrections to photon counting distributions, *Phys. Rev. Lett.*, 16, 589–592, doi:10.1103/PhysRevLett.16.589, 1966. 7745

Kanitz, T., Seifert, P., Ansmann, A., Engelmann, R., Althausen, D., Casiccia, C., and Rohwer, E. G.: Contrasting the impact of aerosols at northern and southern midlatitudes on heterogeneous ice formation, *Geophys. Res. Lett.*, 38, L17802, doi:10.1029/2011GL048532, 2011. 7740

Kanitz, T., Ansmann, A., Engelmann, R., and Althausen, D.: North-south cross sections of aerosol layering over the Atlantic Ocean from multiwavelength Raman/polarization lidar during Polarstern cruises, *J. Geophys. Res.*, 118, 2642–2655, doi:10.1002/jgrd.50273, 2013. 7740, 7747

Kanitz, T., Engelmann, R., Heinold, B., Skupin, A., and Ansmann, A.: Tracking the Saharan Air Layer with shipborne lidar across the tropical Atlantic, *Geophys. Res. Lett.*, 41, 1044–1050, doi:10.1002/2013GL058780, 2014. 7754, 7756

Liu, Z., Kuehn, R., Vaughan, M., Winker, D., Omar, A., Powell, K., Trepte, C., Hu, Y., and Hostetler, C.: The CALIPSO cloud and aerosol discrimination: version 3 algorithm and test

Raman Lidar Polly^{XT}:
the neXT generation

R. Engelmann et al.

Title Page

Abstract

Introduction

Conclusions

References

Tables

Figures

◀

▶

◀

▶

Back

Close

Full Screen / Esc

Printer-friendly Version

Interactive Discussion



results, in: Proceedings of the 25th International Laser Radar Conference, 5–9 July 2010, St.-Petersburg, Russia, ISBN978-5-94458-109-9, 1245–1248, 2010. 7747

Mamouri, R. E. and Ansmann, A.: Fine and coarse dust separation with polarization lidar, Atmos. Meas. Tech., 7, 3717–3735, doi:10.5194/amt-7-3717-2014, 2014. 7747

5 Mattis, I., Ansmann, A., Althausen, D., Jaenisch, V., Wandinger, U., Müller, D., Arshinov, Y. F., Bobrovnikov, S. M., and Serikov, I. B.: Relative-humidity profiling in the troposphere with a Raman lidar, Appl. Optics, 41, 6451–6462, 2002. 7747

Mattis, I., Tesche, M., Grein, M., Freudenthaler, V., and Müller, D.: Systematic error of lidar profiles caused by a polarization-dependent receiver transmission: quantification and error correction scheme, Appl. Optics, 48, 2741–2751, 2009. 7749

10 Müller, D., Wandinger, U., and Ansmann, A.: Microphysical particle parameters from extinction and backscatter lidar data by inversion with regularization: theory, Appl. Optics, 38, 2346–2357, doi:10.1364/AO.38.002346, 1999. 7740

Müller, D., Ansmann, A., Mattis, I., Tesche, M., Wandinger, U., Althausen, D., and Pisani, G.: Aerosol-type-dependent lidar ratios observed with Raman lidar, J. Geophys. Res., 112, D16202, doi:10.1029/2006JD008292, 2007. 7740, 7755

15 Omar, A. H., Winker, D. M., Kittaka, C., Vaughan, M. A., Liu, Z., Hu, Y., Treppe, C. R., Rogers, R. R., Ferrare, R. A., Lee, K. P., Kuehn, R. E., and Hostetler, C. A.: The CALIPSO automated aerosol classification and lidar ratio selection algorithm, J. Atmos. Ocean. Tech., 26, 1994–2014, doi:10.1175/2009JTECHA1231.1, 2009. 7747

20 Pappalardo, G., Amodeo, A., Apituley, A., Comeron, A., Freudenthaler, V., Linné, H., Ansmann, A., Bösenberg, J., D'Amico, G., Mattis, I., Mona, L., Wandinger, U., Amiridis, V., Alados-Arboledas, L., Nicolae, D., and Wiegner, M.: EARLINET: towards an advanced sustainable European aerosol lidar network, Atmos. Meas. Tech., 7, 2389–2409, doi:10.5194/amt-7-2389-2014, 2014. 7738, 7739

25 Preißler, J., Wagner, F., Guerrero-Rascado, J. L., and Silva, A. M.: Two years of free-tropospheric aerosol layers observed over Portugal by lidar, J. Geophys. Res., 118, 3676–3686, doi:10.1002/jgrd.50350, 2013. 7740, 7747

30 Reichardt, J., Baumgart, R., and McGee, T. J.: Three-signal method for accurate measurements of depolarization ratio with lidar, Appl. Optics, 42, 4909–4913, doi:10.1364/AO.42.004909, 2003. 7750

**Raman Lidar Polly^{XT}:
the neXT generation**

R. Engelmann et al.

Title Page

Abstract

Introduction

Conclusions

References

Tables

Figures



Back

Close

Full Screen / Esc

Printer-friendly Version

Interactive Discussion



Sakai, T., Nagai, T., Zaizen, Y., and Mano, Y.: Backscattering linear depolarization ratio measurements of mineral, sea-salt, and ammonium sulfate particles simulated in a laboratory chamber, *Appl. Optics*, 49, 4441–4449, doi:10.1364/AO.49.004441, 2010. 7748

Sassen, K.: Meteorology: dusty ice clouds over Alaska, *Nature*, 434, 456, doi:10.1038/434456a, 2005. 7747

Schmidt, J., Wandinger, U., and Malinka, A.: Dual-field-of-view Raman lidar measurements for the retrieval of cloud microphysical properties, *Appl. Optics*, 52, 2235–2247 doi:10.1364/AO.52.002235, 2012. 7757

Seifert, P., Ansmann, A., Mattis, I., Wandinger, U., Tesche, M., Engelmann, R., Müller, D., Pérez, C., and Haustein, K.: Saharan dust and heterogeneous ice formation: eleven years of cloud observations at a central European EARLINET site, *J. Geophys. Res.*, 115, 2156–2202, doi:10.1029/2009JD013222, 2010. 7744

Simeonov, V., Larcheveque, G., Quaglia, P., van den Bergh, H., and Calpini, B.: Influence of the photomultiplier tube spatial uniformity on lidar signals, *Appl. Optics*, 38, 5186–5190, doi:10.1364/AO.38.005186, 1999. 7743

Tesche, M., Ansmann, A., Müller, D., Althausen, D., Engelmann, R., Freudenthaler, V., and Groß, S.: Vertically resolved separation of dust and smoke over Cape Verde using multiwavelength Raman and polarization lidars during Saharan Mineral Dust Experiment 2008, *J. Geophys. Res.*, 114, D13202, doi:10.1029/2009JD011862, 2009. 7747, 7755

Tesche, M., Groß, S., Ansmann, A., Müller, D., Althausen, D., Freudenthaler, V., and Esselborn, M.: Profiling of Saharan dust and biomass-burning smoke with multiwavelength polarization Raman lidar at Cape Verde, *Tellus B*, 63, 16360, doi:10.3402/tellusb.v63i4.16360, 2011. 7755

Tesche, M., Glantz, P., Johansson, C., Norman, M. G., Hiebsch, A., Seifert, P., Ansmann, A., Engelmann, R., and Althausen, D.: Volcanic ash over Scandinavia originating from the Grimsvötn eruptions in May 2011, *J. Geophys. Res.*, 117, D09201, doi:10.1029/2011JD017090, 2012. 7738

Wandinger, U.: Raman Lidar, in: *Lidar – Range-Resolved Optical Remote Sensing of the Atmosphere*, edited by: Weitkamp, C., Springer Series in Optical Sciences, New York, 241–271, doi:10.1007/0-387-25101-4_9, 2005. 7746

Wandinger, U. and Ansmann, A.: Experimental determination of the lidar overlap profile with Raman lidar, *Appl. Optics*, 41, 511–514, 2002. 7754

**Raman Lidar Polly^{XT}:
the neXT generation**

R. Engelmann et al.

Title Page

Abstract

Introduction

Conclusions

References

Tables

Figures



Back

Close

Full Screen / Esc

Printer-friendly Version

Interactive Discussion



- Wandinger, U., Seifert, P., Engelmann, R., Bühl, J., Wagner, J., Schmidt, J., Pospichal, B., Baars, H., Hiebsch, A., Kanitz, T., Skupin, A., Pfitzenmaier, L., Heese, B., Althausen, D., and Ansmann, A.: Observations of aerosol-cloud-turbulence interaction with integrated remote-sensing instrumentation, in: Proceedings of the 9th International Symposium on Tropo-
spheric Profiling, edited by: Cimini, D., Di Girolamo, P., Marzano, F. S., and Rizi, V., L'Aquila, Italy, 3–7 September 2012, doi:10.12898/ISTP9prc, 2012. 7739
- Whiteman, D. N.: Examination of the traditional Raman lidar technique. I. Evaluating the temperature-dependent lidar equations, Appl. Optics, 42, 2571–2592, doi:10.1364/AO.42.002571, 2003. 7745
- Winker, D. M., Vaughan, M. A., Omar, A., Hu, Y., Powell, K. A., Liu, Z., Hunt, W. H., and Young, S. A.: Overview of the CALIPSO mission and CALIOP data processing algorithms, J. Atmos. Ocean. Tech., 26, 2310–2323, doi:10.1175/2009JTECHA1281.1, 2009. 7738

Raman Lidar Polly^{XT}:
the neXT generation

R. Engelmann et al.

Table 1. Measurement capabilities of the different Polly systems at UV (355 nm), VIS (532 nm), and IR (1064 nm) wavelengths. Water-vapor (W/V) channels and absolute calibration of the depolarization channels (δ -cal.) have been installed in most of the systems. The four most recent systems include a near-range (N/R) telescope in addition.

System	UV	VIS	IR	W/V	δ -cal.	N/R
Prototype		α, β				
IFT*	α, β	α, β, δ	β	x	x	
TROPOS*	α, β, δ	α, β, δ	β	x	x	
FMI	α, β	α, β, δ	β	x	x	
CGE	α, β	α, β, δ	β			
NIER		α, β, δ				
OCEANET	α, β, δ	α, β, δ	β	x	x	x
UW	α, β, δ	α, β, δ	β	x	x	x
NOA	α, β, δ	α, β, δ	β	x	x	x
DWD	α, β	α, β, δ	β		x	x

*The system labeled IFT (former abbreviation of the Institute for Tropospheric Research) was upgraded with an additional UV depolarization channel and the new data acquisition in January 2015 and is now labeled TROPOS.

Title Page

Abstract

Introduction

Conclusions

References

Tables

Figures

◀

▶

◀

▶

Back

Close

Full Screen / Esc

Printer-friendly Version

Interactive Discussion



Table 2. Specification of the portable Raman lidar Polly^{XT}. N/R denotes the near-range receiver unit.

Size	1.8 m × 1.7 m × 0.8 m
Weight	500 kg, movable by 4 wheels
Power	≈ 2 × 1.5 kW (lidar and air condition)
Transmitter:	
Laser	Inlite III (Continuum) with external SHG and THG. Power: 180 mJ (1064 nm), 110 mJ (532 nm), 60 mJ (355 nm)
Polarization	s-pol (with respect to the beamsplitters), cleaned by Glan-Laser polarizer
Beam expander	8×, achromatic
Beam divergence	< 0.2 mrad
Receiver:	
Telescope	Newtonian: $d = 0.3$ m, $f = 0.9$ m N/R: achromat, $d = 0.05$ m, $f = 0.25$ m
Field of view	1, 2.2 mrad (N/R)
Channels at/ Bandwidth (FWHM)	1064/1.0, 607/0.3, 607 (N/R)/0.3, 532/1.0, 532 (cross)/1.0, 532 (N/R)/1.0 407/1.0, 387/0.3, 355/1.0, 355 (cross)/1.0 nm
Photomultiplier	Hamamatsu P10721-110 Hamamatsu R3236 (only at 1064 nm)
Beam alignment	triggered camera
Signal acquisition	800 MHz photon counters, 7.5 m, pretrigger, up to 48 km

Raman Lidar Polly^{XT}: the neXT generation

R. Engelmann et al.

Title Page

Abstract

Introduction

Conclusions

References

Tables

Figures



Back

Close

Full Screen / Esc

Printer-friendly Version

Interactive Discussion



**Raman Lidar Polly^{XT}:
the neXT generation**

R. Engelmann et al.

Title Page

Abstract

Introduction

Conclusions

References

Tables

Figures



Back

Close

Full Screen / Esc

Printer-friendly Version

Interactive Discussion

**Table 3.** Specification of the new data acquisition hardware as applied in Polly^{XT}.

Number of channels	8
Height resolution	7.5 m
Maximum altitude	≈ 40 km
Pre-trigger	≈ 256 bins
Electronic count rate	> 800 MHz
Overall dead time	2–3 ns (varies with each PMT module) 3–4 ns (R3236 PMT at 1064 nm channel)

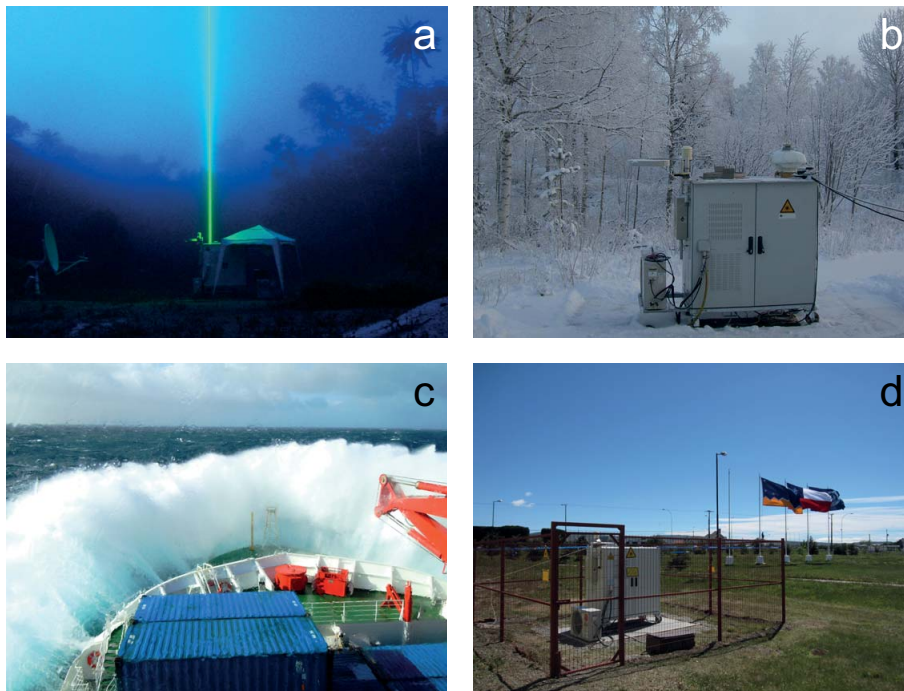


Figure 1. Autonomous measurements of Polly^{XT} in **(a)** the Amazon basin, 2° S, at > 90 % relative humidity, **(b)** at Kuopio, Finland, 62° N, in winter, **(c)** aboard the RV *Polarstern* during 8 m ground swell, and **(d)** at the southern edge of Latin America, Punta Arenas, Chile, 52° S.

Raman Lidar Polly^{XT}: the neXT generation

R. Engelmann et al.

Title Page

Abstract

Introduction

Conclusions

References

Tables

Figures

◀

▶

◀

▶

Back

Close

Full Screen / Esc

Printer-friendly Version

Interactive Discussion



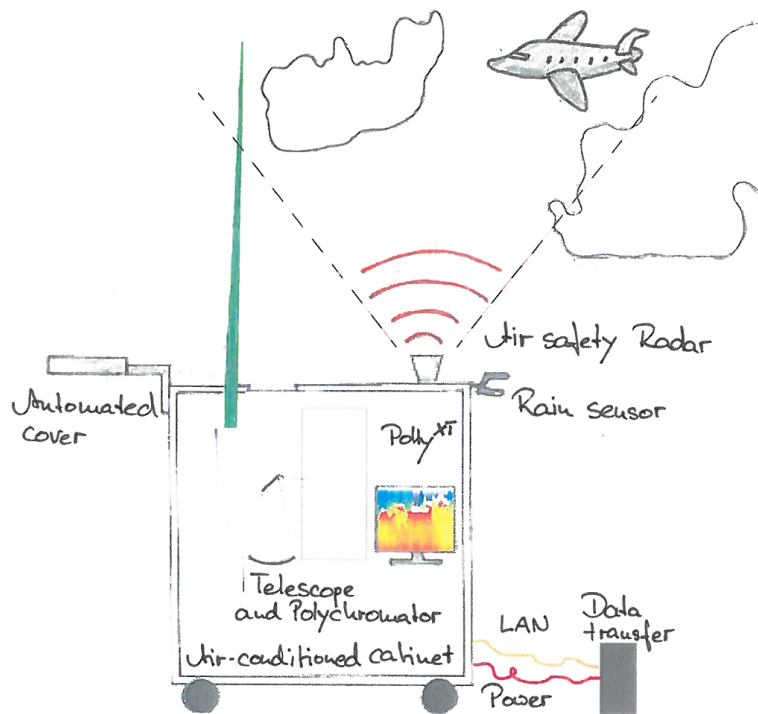


Figure 2. The general concept of Polly. These unattended aerosol Raman lidars have already been deployed worldwide for campaigns with periods on the order of one year. They are completely controlled via remote access, automatically shut down in events of rain, can be connected to an air-safety radar, and transfer the data to a centralized data server where the data are archived and automatically evaluated. In this way, issues with data quality can be easily identified and the users are informed. The system's mass is approximately 500 kg, but they can be easily moved on the four wheels.

Raman Lidar Polly^{XT}: the neXT generation

R. Engelmann et al.

Title Page

Abstract

Introduction

Conclusions

References

Tables

Figures

◀

▶

◀

▶

Back

Close

Full Screen / Esc

Printer-friendly Version

Interactive Discussion



Raman Lidar Polly^{XT}: the neXT generation

R. Engelmann et al.

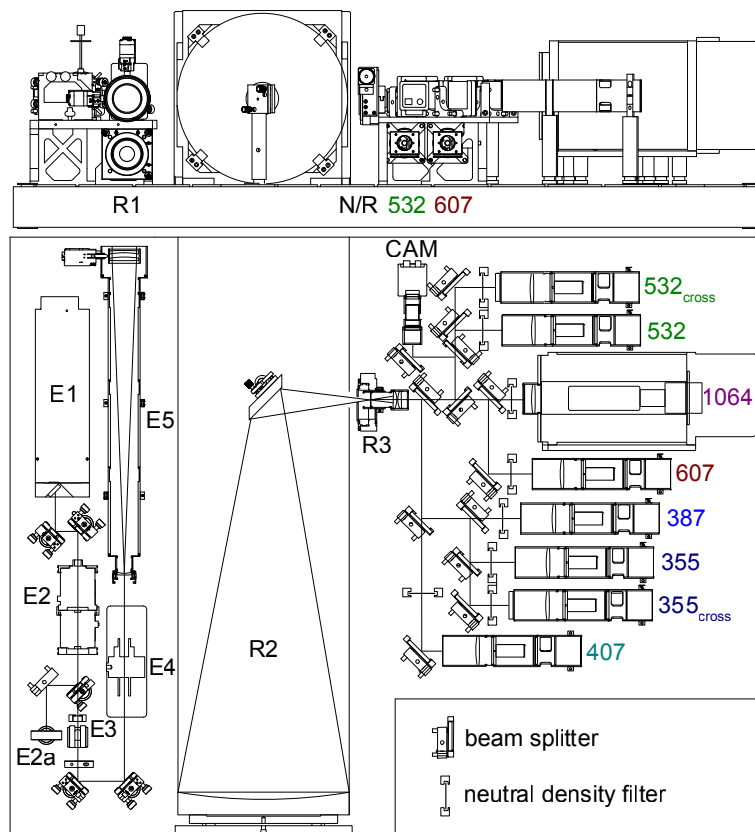


Figure 3. The optical setup of Polly^{XT}_OCEANET. The upper part displays a top view and the lower part the front view of the system. Details are explained in the text.

Title Page	
Abstract	Introduction
Conclusions	References
Tables	Figures
◀	▶
◀	▶
Back	Close
Full Screen / Esc	
Printer-friendly Version	
Interactive Discussion	



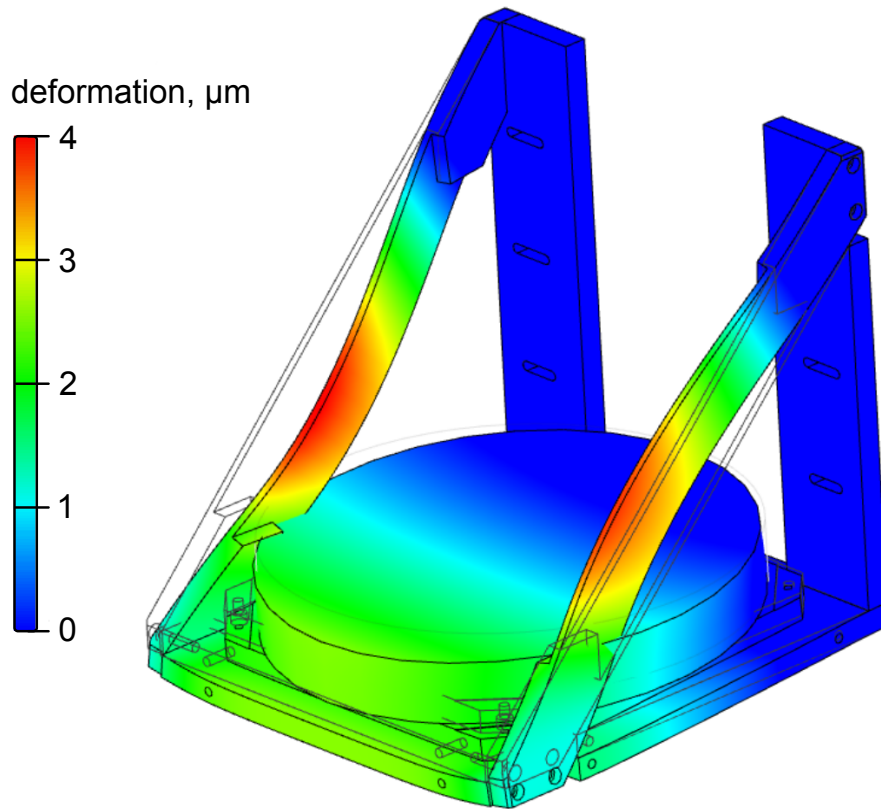


Figure 4. FEM calculations of the maximal deformation of the mounting of the primary mirror during the vertical adjustment in the cabinet. The deformation intensity is given by the color code.

Raman Lidar Polly^{XT}: the neXT generation

R. Engelmann et al.

Title Page

Abstract

Introduction

Conclusions

References

Tables

Figures

◀

▶

◀

▶

Back

Close

Full Screen / Esc

Printer-friendly Version

Interactive Discussion



Raman Lidar Polly^{XT}:
the neXT generation

R. Engelmann et al.

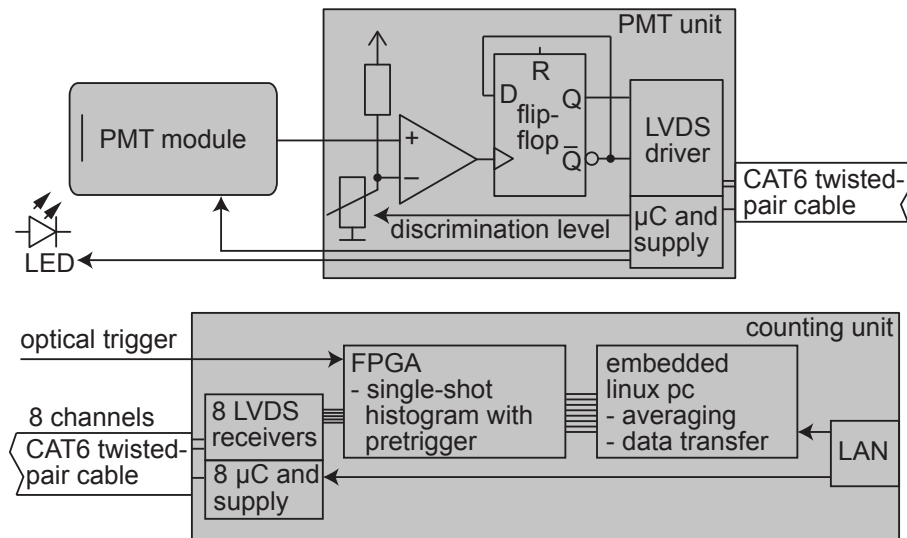


Figure 5. Scheme of the eight-channel data-acquisition system. Each PMT and the discrimination electronics are constructed as a fixed unit (top panel). The photon pulses from a maximum of eight detector units are then digitally transferred to the counting unit (bottom panel) where the histograms are processed, averaged, and can be obtained by the measurement PC via a LAN connection.

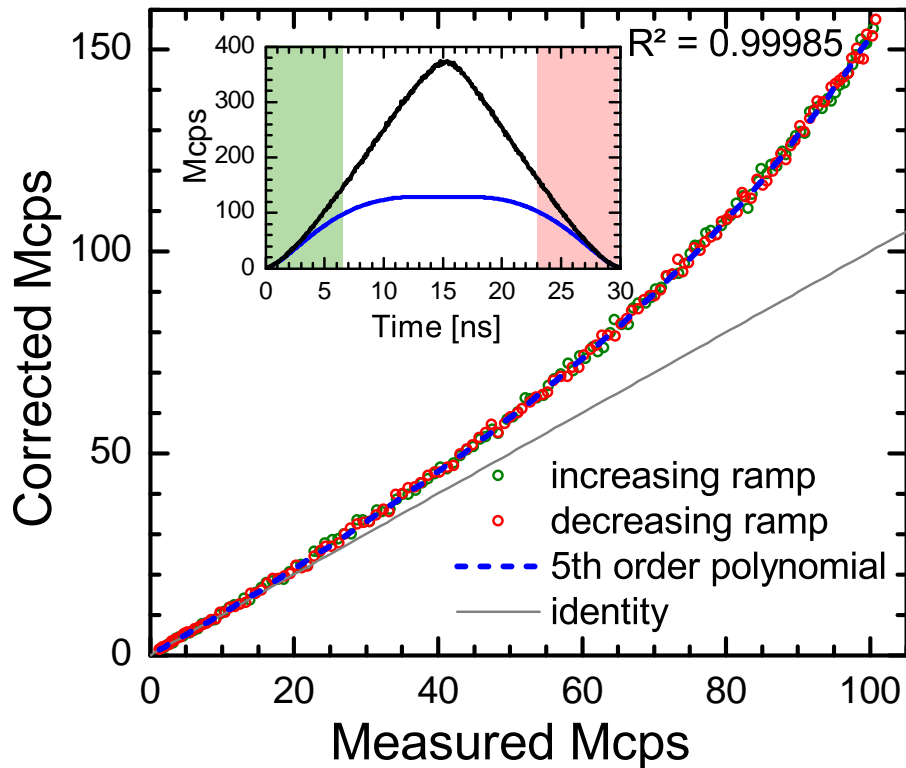


Figure 6. Measurement of dead-time effects: a defined light ramp is detected with high and low (by use of an attenuator) count rates, respectively. The inset shows the light ramps with high count rates (blue) and with low count rates (black) but scaled (by a factor of approx. 100) so that both curves match identity at count rates < 10 Mcps. The main graph shows the resulting correlation and a 5th-order polynomial fit which is directly applied for dead-time correction.

Title Page	
Abstract	Introduction
Conclusions	References
Tables	Figures
◀	▶
◀	▶
Back	Close
Full Screen / Esc	
Printer-friendly Version	
Interactive Discussion	



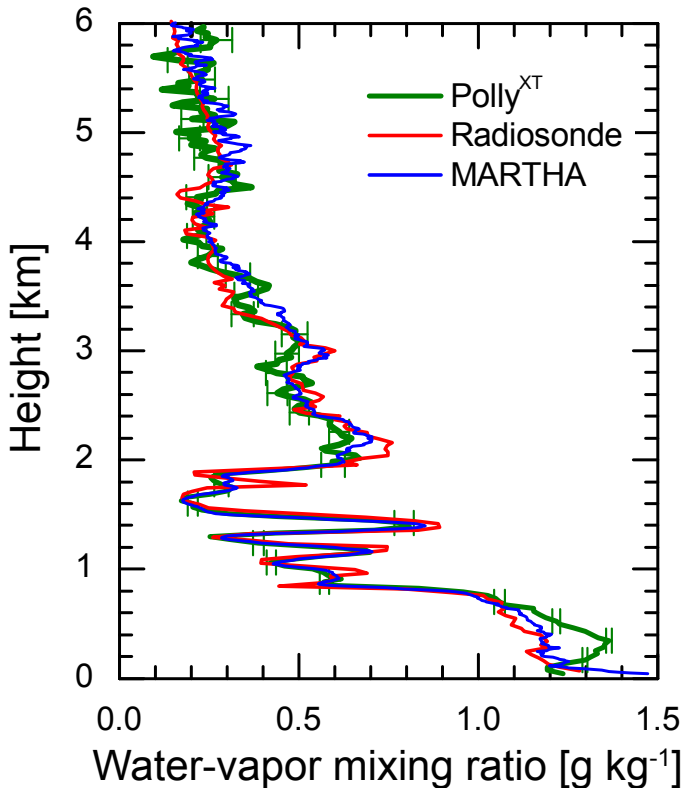


Figure 7. 90 min mean profiles of the water-vapor mixing ratio as determined with Polly (green, 30 m vertical smoothing up to 2 km height, 60 m above), a co-located radiosonde (red), and coincident measurements of the EARLINET Raman lidar MARTHA (blue, resolution 30 m) at Leipzig on 10 February 2012 (19:00–20:30 UTC).

**Raman Lidar Polly^{XT}:
the neXT generation**

R. Engelmann et al.

Title Page	
Abstract	Introduction
Conclusions	References
Tables	Figures
◀	▶
◀	▶
Back	Close
Full Screen / Esc	
Printer-friendly Version	
Interactive Discussion	



Raman Lidar Polly^{XT}:
the neXT generation

R. Engelmann et al.

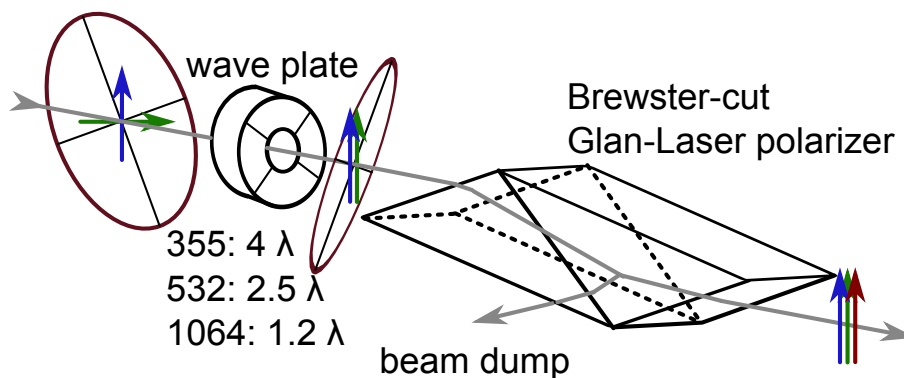


Figure 8. Wave plate and polarizer setup used to generate highly linear-polarized light at three wavelengths. The different polarization states after SHG and THG are matched by the wave plate and afterwards purified by the polarizer.

Title Page

Abstract

Introduction

Conclusions

References

Tables

Figures

◀

▶

◀

▶

Back

Close

Full Screen / Esc

Printer-friendly Version

Interactive Discussion



**Raman Lidar Polly^{XT}:
the neXT generation**

R. Engelmann et al.

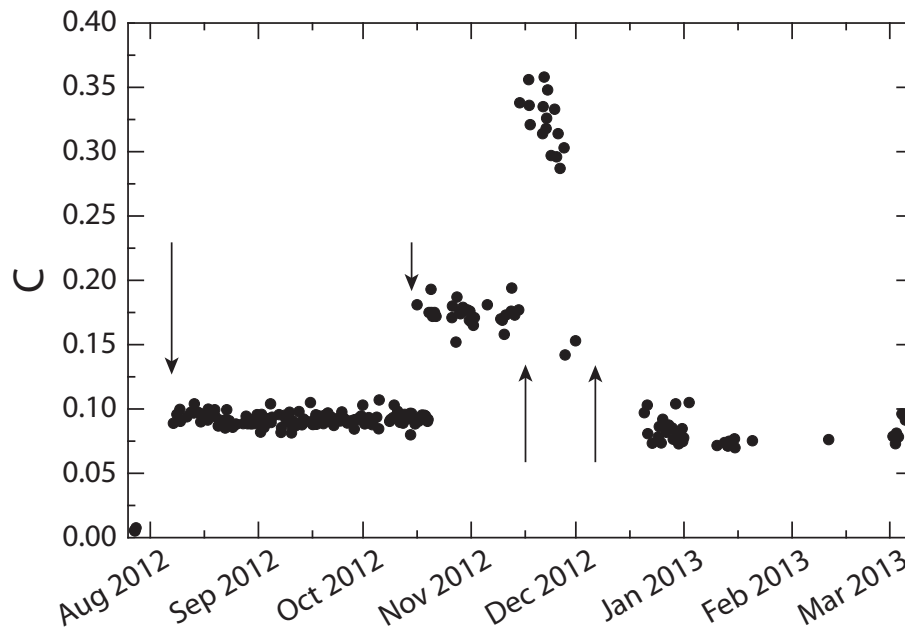


Figure 9. Time series of the routinely determined calibration constant C during measurements of Polly^{XT}_IFT from August 2012 to April 2013. Arrows denote adjustments of the neutral-density filters. Gaps in the time series are caused by measurement interruptions during bad weather.

[Title Page](#)[Abstract](#)[Introduction](#)[Conclusions](#)[References](#)[Tables](#)[Figures](#)[◀](#)[▶](#)[◀](#)[▶](#)[Back](#)[Close](#)[Full Screen / Esc](#)[Printer-friendly Version](#)[Interactive Discussion](#)

**Raman Lidar Polly^{XT}:
the neXT generation**

R. Engelmann et al.

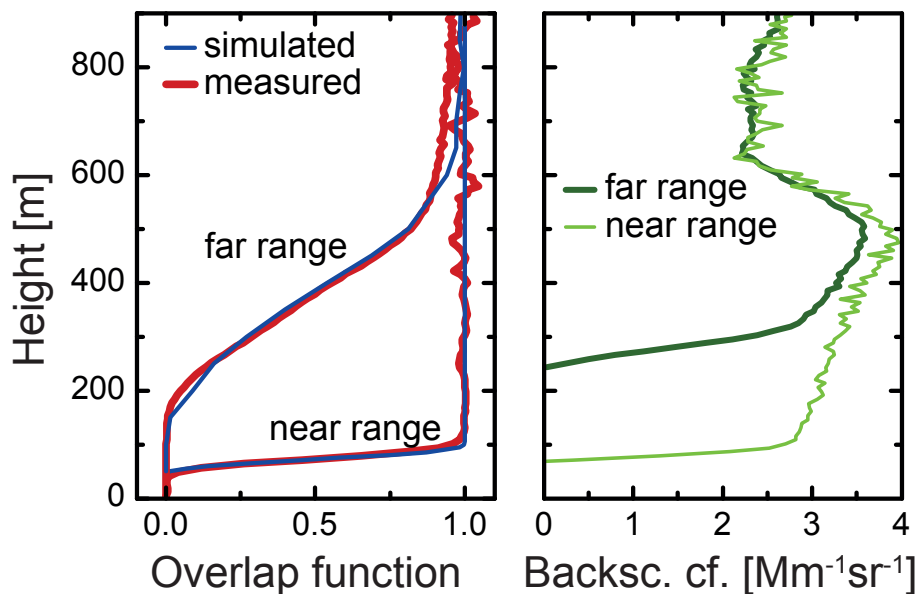


Figure 10. Left: simulated (thin, blue) and experimentally determined (thick, red) overlap functions of far-range and near-range telescopes of Polly^{XT}_OCEANET. Right: backscatter coefficient at 532 nm derived with the Klett method (lidar ratio: 30 sr, no overlap correction performed) from far-range (thick, green) and near-range (thin, light green) signal from a measurement aboard RV *Meteor* on 05 May 2013 from 22:00–22:30 UTC.

[Title Page](#)[Abstract](#)[Introduction](#)[Conclusions](#)[References](#)[Tables](#)[Figures](#)[◀](#)[▶](#)[◀](#)[▶](#)[Back](#)[Close](#)[Full Screen / Esc](#)[Printer-friendly Version](#)[Interactive Discussion](#)

Raman Lidar Polly^{XT}:
the neXT generation

R. Engelmann et al.

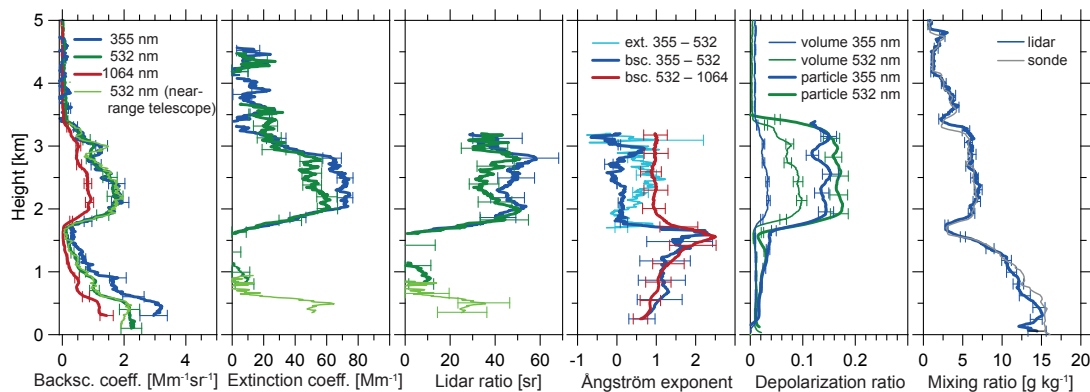


Figure 11. Optical and meteorological products obtained on board of RV *Meteor* between 23:15 and 23:58 UTC on 09 May 2013. A Saharan dust plume above the marine boundary layer was tracked. Shown are from left to right the particle backscatter coefficient, the particle extinction coefficient, the corresponding lidar ratios and Ångström exponents, the volume and particle linear depolarization ratios, and the water-vapor mixing ratio.

Title Page

Abstract

Introduction

Conclusions

References

Tables

Figures



Back

Close

Full Screen / Esc

Printer-friendly Version

Interactive Discussion

